JOURNAL OF SPACECRAFT AND ROCKETS
Vol. 31, No. 3, May–June 1994

Minimum-Drag Axisymmetric Bodies in the Supersonic/Hypersonic Flow Regimes

W. H. Mason* and Jaewoo Lee†
Virginia Polytechnic Institute and State University, Blacksburg, Virginia 24061

A study of minimum-drag body shapes was conducted over a Mach range from 3 to 12. Numerical results show that power-law bodies result in low-drag shapes, where the power $n = 0.69$ ($l/d = 3$) or $n = 0.70$ ($l/d = 5$) shapes have lower drag than theoretical minimum results ($n = 0.75$ or 0.66, depending on the particular form of the theory). To evaluate the results, a numerical analysis was made, including viscous effects and the effect of a gas model. None of these considerations altered the conclusions. The Hayes minimum-drag body was analyzed and had a higher drag than the optimum power-law body.

Nomenclature

C_D = drag coefficient based on the maximum cross-sectional area
C_f = skin-friction coefficient
C_p = pressure coefficient
d = body diameter at the base
i = marching plane index
K_{SH} = unified supersonic-hypersonic similarity parameter, $(M_\infty^2 - 1)^{0.5}/(l/d)$
l = body length
M_∞ = freestream Mach number
n = power-law exponent
r = body radius
T = temperature at the body surface
T_{ref} = freestream temperature
x, y, z = physical coordinates
θ = circumferential angle

Introduction

CONSIDERATION is being given to both the High Speed Civil Transport (HSCT) and the X-30 National Aerospace Plane (NASP) to initiate a new era of advanced vehicles.[1] Although both supersonic and hypersonic configurations have been studied seriously in the past, the possibility of such configurations becoming practical relies on achieving the potential of advanced propulsion and materials technology, as well as of aerodynamic design. Based on the history of propulsion advances, we expect that the first generation of these advanced propulsion systems will not have reached full maturity and that performance will be marginal. Thus, not only is the propulsion system crucial, but also a maximum effort is required to minimize the airframe drag.

Minimum-drag bodies have been studied extensively both for supersonic and hypersonic flight, with an entire book[2] devoted to the subject during a previous period of intense interest. At that time only simplified theoretical analyses were practical to find minimum-drag shapes. Subsequently, minimum-drag shapes received less attention, while other design considerations dominated the aerodynamic design problem. With sustained hypersonic cruise flight once again of interest, the importance of achieving low drag dictates that additional work be done in this area.

Since the original minimum-drag shapes were derived, a revolution has taken place in aerodynamics. Advanced computational methods, now applied routinely to analyze body shapes, can be used to re-examine the classical minimum-drag shapes. The purpose of this paper is to clarify the historical results through a computational examination of several of the previously proposed minimum-drag shapes using an advanced computational method. Our interest is in the high supersonic/moderate hypersonic speed regime ($M_\infty \approx 3$–12, Mach numbers of interest for low drag and, hence, slender shapes), where we expect that neither the linearized supersonic nor the Newtonian hypersonic analysis will be accurate. This is precisely the Mach number range of interest in a number of current aircraft studies.

The following section reviews a number of classical investigations and the shapes that have been found to have minimum drag under various assumptions. We then define the computational investigation to be conducted, the computational method, and the results. Specific attention is paid to numerical accuracy. Results for the so-called "hypersonic power-law bodies" are presented, including a detailed examination of both the blunt-nose effects and the effects of using an equilibrium-air model. A parabolized Navier-Stokes calculation is presented to examine viscous effects, and then results for one other body of interest are presented. The results of the study provide a rigorous basis on which to draw conclusions about the selection of the best shapes for high supersonic/hypersonic speed vehicles.

Review of Minimum-Drag Studies

For cases where analytic theories are available and valid, minimum-drag shapes have been determined theoretically for a wide range of constraint conditions. Analytic theories are available for both linearized supersonic flow and for hypersonic flow when either Newtonian theory or small disturbance theory is valid. Figure 1 presents a summary of the situation by Fink[3] and is based on his figure. Minimum-drag bodies found using several analytic and numerical results are shown. The figure also illustrates the large gap between the regions where analytic solutions are available. This gap occurs for values of the Mach number similarity parameter between about 0.6 and 4.0. For NASA's conical aerospace plane concept,[4] this gap corresponds to the Mach range of $M_\infty = 3.48$–22.2 based on the fineness ratio to the maximum diameter (or $M_\infty = 4.43$–28.8 for the entire length). Thus this gap occurs precisely where much of the future high-speed vehicle flight will take place.

Table 1 presents a summary of the various classical minimum-drag shapes of interest here. These shapes correspond to

Presented as Paper 90-3072 at the AIAA 8th Applied Aerodynamics Conference, Portland, OR, Aug. 20–22, 1990; received Oct. 2, 1990; revision received Aug. 21, 1991; accepted for publication June 2, 1992.

*Associate Professor, Department of Aerospace and Ocean Engineering. Associate Fellow AIAA.

†Graduate Research Assistant; currently Senior Researcher, Agency for Defense Development, Republic of Korea. Member AIAA.

Table 1 Summary of the various minimum drag shapes

Name	Theory	Mach no. range	Body shape	$C_D\ (l/d)^2$
Karman ogive (1935)	Slender body	Low-moderate supersonic	Infinite slope and zero radius at the nose, zero slope at the base	1.0
Parker (1955)	Linearized supersonic	Low-moderate supersonic	Pointed nose nonzero body slope at the base	0.75–0.925
Eggers et al. (1957)	Newtonian impact	∞	Power-law body, n = 0.75	0.352
Hayes (1959)	Newtonian Busemann	∞	Power-law body, n = 0.75 initially and 1/3 afterward	0.288
Cole (1957)	Newtonian Busemann, slender body	∞	Power-law body, n = 0.66	0.334
Fink (1966)	Hypersonic small-disturbance theory	Hypersonic	Depends on Mach no.	0.367–0.50

bodies of given length and diameter (the case that most closely corresponds to actual aircraft design requirements for current supersonic aircraft) and their maximum cross-sectional area at the base (which has been the classical case of interest in hypersonic flow). Perhaps the most unexpected feature of the classical results for both supersonic and hypersonic minimum-drag bodies of given length and diameter is that the bodies are not pointed. If the length is unspecified, a pointed tip will result and, in fact, be cusped. This tip is unsuitable for high-speed cruise vehicles for both structural and aerodynamic heating reasons.

Analytical Studies

In the case of supersonic flow, the von Kármán ogive[2] was derived using slender-body theory. The derivation requires that the body slope at the base be zero. The resulting shape has an infinite nose radius at the leading edge, such that at the exact apex the nose is flat. Consistent with slender-body theory, the body shape and drag exhibit no Mach number dependence.

Parker[5] derived the minimum-drag shape using linearized supersonic theory. That minimum-drag body was pointed at the nose, but with an initial slope equal to the Mach cone angle. In his case this was the maximum slope that the theoretical analysis allowed. Thus the slope is large for moderate supersonic speeds for which the theory is valid. Parker's analysis didn't require that the body slope at the base be zero, and a nonzero slope resulted. As shown in Fig. 1, his results exhibit a Mach number dependence, predict a body with less drag than the von Kármán ogive, and are valid for small values of the similarity parameter.

At hypersonic speeds Eggers et al.[6] used the Newtonian impact theory to show that a small finite radius exists at the

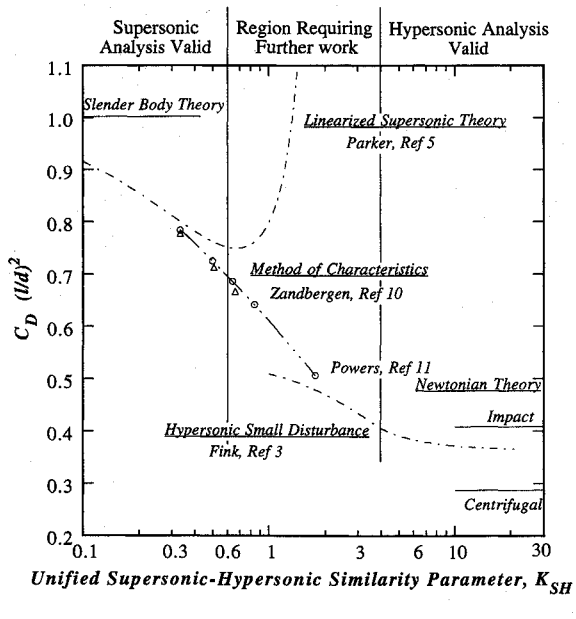

Fig. 1 Demonstration of gap between linearized supersonic and hypersonic minimum-drag body theory (Fink[3]).

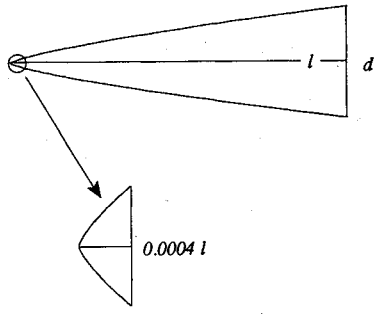

Fig. 2 Details of blunt-nose shape.

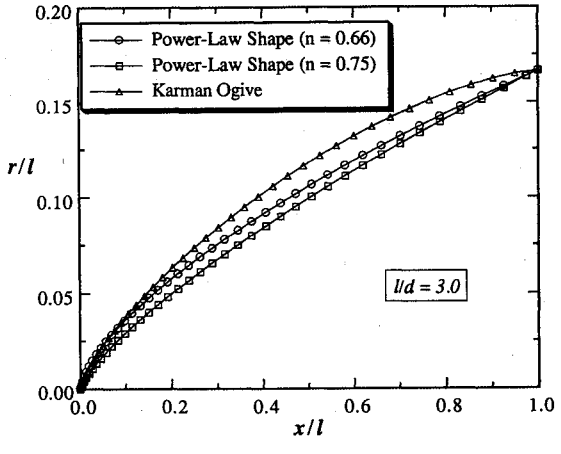

Fig. 3 Comparison of minimum-drag shapes.

nose of the minimum-drag body. The initial body slope at the edge of the flat surface is 45 deg. The length scale of this flat surface is extremely small, and solutions obtained on computational meshes appropriate for the solution over the entire body do not reveal the features of this region. The analysis in both supersonic and hypersonic cases demonstrates that when length is held fixed, a high pressure applied over the differential area $r dr d\theta$ is acceptable at the nose, where $r \to 0$. This allows reduced slopes and hence reduced drag forces over those parts of the body where the differential area is larger. In addition, Eggers et al.[6] showed that a power-law body of the form $r \sim x^n$ closely approximated the minimum-drag shape obtained analytically when $n = 3/4$. Figure 2 illustrates the extremely small scale of the blunt region of the body.

A slightly different shape is obtained if the so-called Busemann correction is introduced into the hypersonic flow theory. This was done by Hayes and Probstein.[7] In this case the shock wave is allowed to separate from the body at some distance along the surface. The drag predicted with this shape is less than the value determined by Eggers et al.,[6] as shown in Table 1. The Hayes shape is found using an $n = 3/4$ power law initially and then using a shape proportional to $(x - x_0)^{1/3}$ aft of a match point x_0. A comparison of the exact Hayes body with the $n = 3/4$ power-law shape is contained in the results section. An alternate derivation of this shape was given by Miele.[8]

The minimum-drag body, including the Busemann correction, results in a body for which the power-law form provides a very close description when $n = 2/3$. Studying the general class of power-law bodies, Cole[9] also found the $n = 2/3$ power-law body to be the minimum-drag shape when the Busemann correction was included.

Figure 3 illustrates the differences between various analytic minimum-drag body shapes. It is clear that for the cases with blunt noses the blunt portion of the body is extremely small relative to the complete shape.

Numerical Studies

In the Mach number (or similarity parameter) region where analytic solutions are not valid, the key contribution has been made by Fink.[3] He examined the gap between the classical linear supersonic and hypersonic theories on the basis of hypersonic small-disturbance approximations to the shock-expansion method. In this region he obtained optimum body shapes using numerical optimization. No a priori assumption was made for the body shape, and the optimum body was obtained as a numerical table of the radii at 25 stations along the length. His results were generally "around" the $n = 3/4$ power-law body shape. Although not given explicitly, the initial vertex angle was large. In using the shock-expansion method, Fink was constrained by the theory to obtain shapes for which the initial nose angle resulted in an attached shock.

Two other sets of results are contained in Fig. 1. Zandbergen[10] computed numerical solutions for optimum bodies with finite nose angles using the method of characteristics. He started his numerical calculation assuming a conical nose and then allowed the shape to seek an optimum radius distribution aft of the conical starting station. Although he had expected to obtain cusped solutions for the nose shape, the slope was always greatest along the conical nose and began decreasing as soon as it was allowed to change. The implication is that the procedure would have led to very large initial slopes (blunt noses) if the procedure allowed for it. The circular points on the plot were obtained by Powers,[11] who determined optimum shapes for bodies required to have spherical noses. Powers used equilibrium air blunt-body and method-of-characteristics numerical methods. He obtained the optimum shape from a class of spherical nose radii and perturbation polynomials to a baseline body. His optimum shape approximated the 3/4 power-law body with an extremely small spherical cap.

More recently, work has been done by Maestrello and Ting,[12] who used modified Newtonian theory to obtain optimum forebody shapes for the case where the leading-edge radius was specified.

One other significant numerical study of minimum-drag shapes was made by Stivers and Spencer,[13] who used the method of characteristics to compute the drag for four classes of bodies over the Mach number range from 2 to 12. Theirs being one of the few studies of cruise vehicles, they investigated shapes with maximum thickness at the midpoint. The constraint was the use of specified length and volume. The body classes studied included Sears-Haack, parabolic arc, back-to-back von Kármán ogive, and a Miele shape[2] of given surface area and volume rather than length. They included skin-friction and base drag in their analysis. The results indicated that a Sears-Haack body with a slightly cutoff base would be the shape with the lowest total drag. The small blunt nose of the bodies was ignored in the calculation. They did not consider power-law shapes.

Experimental Studies

Several experimental investigations of minimum-drag bodies have been made. Eggers et al.[6] conducted an experimental evaluation of their new shape. Other key investigations were conducted by Perkins et al.,[14] Spencer and Fox,[15] and Fournier et al.[16] In each case the details of the boundary-layer state were not described in enough detail in the report to provide a basis for a rigorous numerical calculation to validate numerical procedures. However, they do provide valuable data for a large range of flow conditions and body shapes. The experimental results essentially confirmed the theoretical analyses.

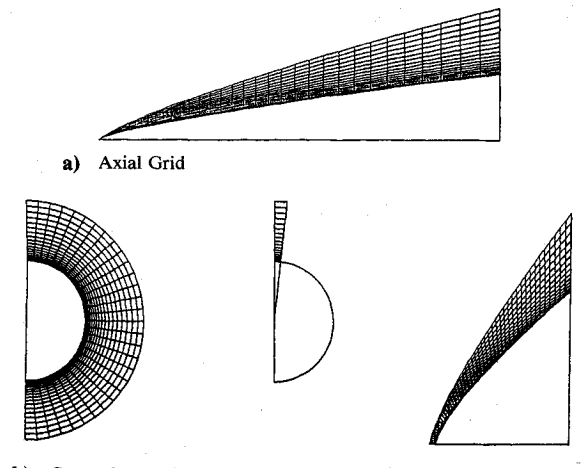

Fig. 4 Computational grid used in present study ($n = 0.75$, $M_\infty = 6.28$, $l/d = 3.0$).

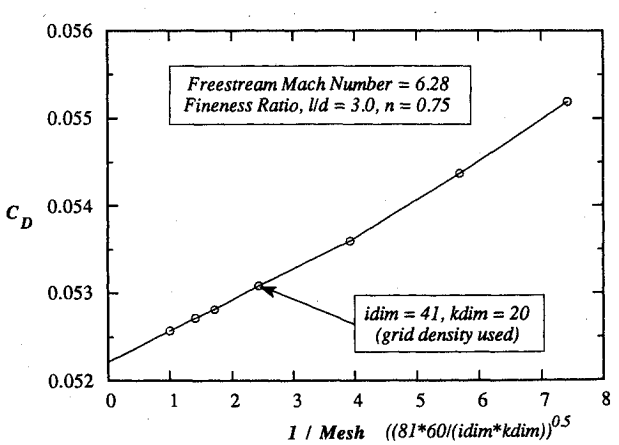

Fig. 5 Convergence of drag with increasing grid density.

Present Numerical Investigation

Although the advanced vehicles being considered will be three dimensional, it appears reasonable to examine the minimum drag of axisymmetric bodies as a logical starting point. In this paper we address the case for which most development has been done in the past: the case of minimum drag for specified length and maximum area, with the maximum area located at the base. First, we evaluate power-law bodies to determine which value of the exponent results in the minimum drag when analyzed using the Euler equations. The results are presented for both perfect-gas and equilibrium-air thermodynamic models over a Mach range from 3 to 12. Using the same method, the Hayes shape is examined to determine the relative drag values. Finally, we evaluate the possible viscous effects by presenting a parabolized Navier-Stokes (PNS) calculation.

Computational Approach and Methodology

We used the modern computational fluid dynamics (CFD) method known as CFL3DE[17] to conduct the study. This code handles both calorically perfect and equilibrium-air gas models and can be used to solve either the Euler equations or the thin-layer Navier-Stokes equations. The method is a cell-centered finite volume scheme that uses upwind/relaxation methods and has been validated by numerous comparisons with data. In one of the validation studies, the PNS mode was evaluated by Huebner et al.[18] by comparison with data at $M_\infty = 7.95$. By considering only axisymmetric bodies and primarily using space-marching techniques, the analysis was performed economically, allowing a thorough investigation of the aerodynamic performance of minimum-drag body shapes.

Grid Selection

In this study of axisymmetric bodies, the CFL3DE code was run as a two-dimensional code using only one "slice" of the full three-dimensional grid in the circumferential direction and enforcing a boundary condition of no circumferential flow gradients. The use of this grid reduced computational time dramatically. The computational grid is compared with the usual grid system in Fig. 4.

Forty-one axial stations were used along the body for the cases presented here, with stations clustered near the nose. This grid was initially determined to be acceptable by comparing drag results obtained with this method and grid with previously computed results. Further grid resolution studies are described later. Twenty points were used between the body and the outer edge of the grid, with clustering near the body, as shown in Fig. 4. Typically, the shock was located approximately three-fourths of the way between the body and outer edge of the grid, but due to the grid stretching, a much higher percentage of the grid points was actually inside the shock.

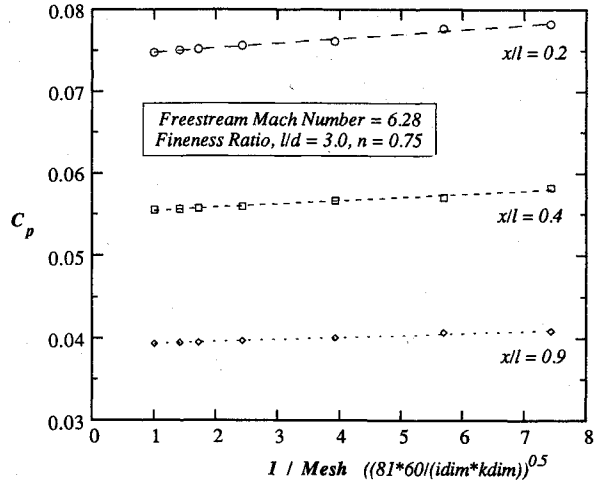

Fig. 6 Convergence of pressure distribution with increasing grid density.

The computations were conducted on the IBM 3090 computer at the Virginia Polytechnic Institute and State University. Typical CPU times were 6 min for calorically perfect gas cases and 6.7 min for cases employing the equilibrium-air gas model.

Numerical Accuracy

A key advantage of the simple axisymmetric model is the ability to carry out detailed convergence studies, providing both confidence and guidance in establishing the required grid resolution for future three-dimensional calculations. An evaluation of the results showed that converged drag values were obtained when the residual was reduced by four orders of magnitude. This criterion was used for all of the results presented.

A grid study was carried out to determine the resolution required to obtain accurate results. The effect of grid density on drag for a typical case is shown in Fig. 5. Figure 6 shows the surface pressure convergence. Note that these results are plotted for the reciprocal of the number of grid points. The origin represents an infinite grid density. Although the drag, as expected, is sensitive to the grid density, the 41×20 grid provides relatively accurate values while allowing a computation economical enough to be made several hundred times.

Results

Computations were made for power-law bodies with values of the exponent from 0.65 to 1.0, over a Mach range from 3 to 12. The Hayes body was also analyzed from Mach 6.28 to 12. The drag coefficients presented are based on the maximum cross-sectional area.

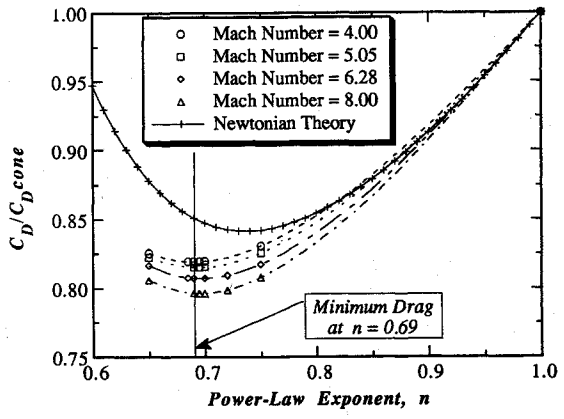

a) Comparison with Newtonian theory

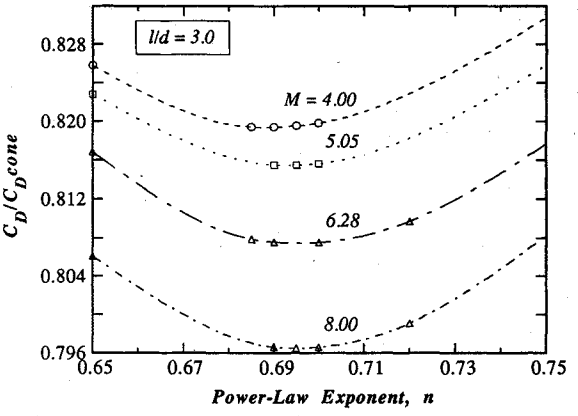

b) Detailed examination of the behavior

Fig. 7 Numerical determination of optimum n for power-law shapes.

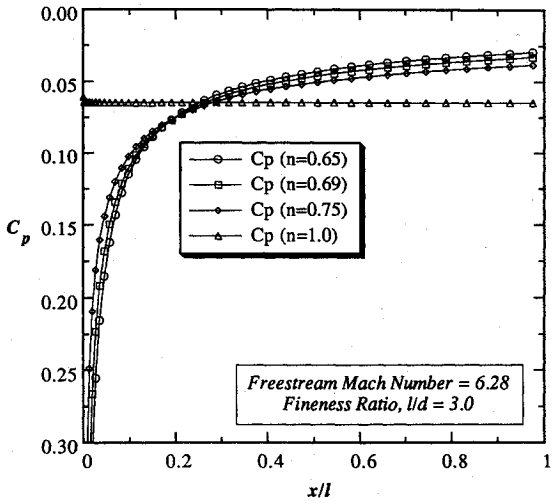

Fig. 8 Pressure distributions for several power-law shapes.

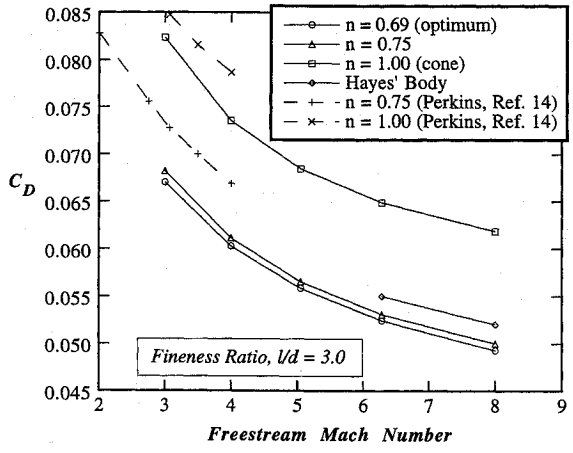

Fig. 9 Mach number effects for several shapes.

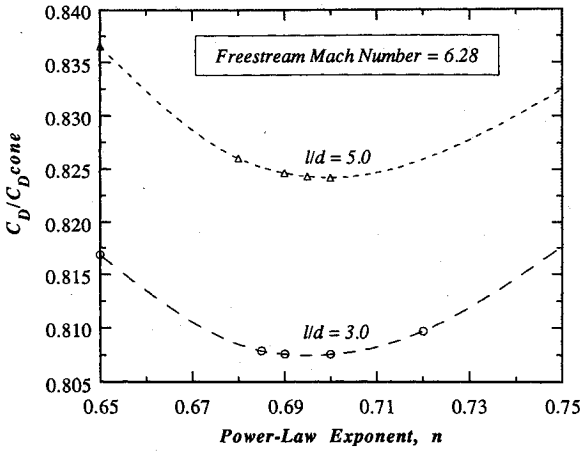

Fig. 10 Comparison of $l/d = 3.0$ and 5.0.

Power-Law Bodies, $l/d = 3$

Using CFL3DE, a parametric study of the inviscid drag of various power-law bodies was conducted for a range of Mach numbers using the calorically and thermally perfect gas model. The baseline for the study was the case of a length to diameter (l/d) of 3. The Mach numbers were selected to correspond to the values at which Eggers et al.[6] conducted experiments. The results are presented in Fig. 7. For comparison, the results from Newtonian theory are also included. The predicted drag is presented compared with the drag of a cone using the same method. Note that the Newtonian minimum occurs near $n = 3/4$, which is well known. The results from CFL3DE predict a bigger reduction in drag than the Newtonian theory, with the minimum occurring at the lower value exponent of approximately 0.69. The theoretical minimum-drag value of power-law bodies occurs at $n = 2/3$ when the Busemann correction is included, and the numerical minimum falls between the pure Newtonian and the Newton-Busemann theory. The drag coefficient decreases with increasing Mach number (as expected based on Fig. 1), but the power-law exponent of the minimum does not vary significantly with Mach number. Figure 7b shows the details around the minimum-drag value. The minimum is mild, but there is a distinct and nontrivial reduction in drag from the $n = 3/4$ case. Finally, note that the trends predicted by Newtonian theory are very accurate for nearly conical bodies but become poor as n becomes significantly different than unity.

Pressure distributions are presented in Fig. 8 for the Mach 6.28 case. The pressure distributions are all very similar for the values of n around the minimum and very different than the cone case. Note that the pressures "cross over" at approximately 20% of the length for the values of n just above and below the optimum. This demonstrates how the minimum arises from a balance of higher pressures near the nose and lower pressures on the aft portion of the body.

Figure 9 presents drag results without normalization by the equivalent cone value for several power-law bodies. Experimental data from Perkins et al.[14] and the results of an analysis of the Hayes body to be discussed later are also included. The Mach number trends and general drag levels are supported by experiment. However, experimental results are difficult to compare directly. The data of Perkins et al.[14] include skin friction not included in the theoretical result. Because of the test Reynolds number variation with Mach number and transition location uncertainties, the experimental data of Eggers et al.[6] are not included in the figure. Without more experimental details it appears inappropriate to compare viscous calculations with this experimental data.

Power-Law Bodies, $l/d = 5$

A limited analysis of the $l/d = 5$ power-law body was made to determine if the change in body slenderness had an effect on the minimum-drag value of the power-law exponent. Figure 10 presents the results of the calculations. It appears that there is, in fact, a small change in the optimum value from $n = 0.69$ to 0.7. Otherwise the trends are similar to the $l/d = 3$ case.

Effects of Viscosity

The possible effect of viscosity on the results was evaluated from parabolized Navier-Stokes solutions using the CFL3D code in the space-marching mode. The computations were made for laminar flow, and the grid was changed from the nominal 41×20 grid to 51×60. The extra radial grid points were tightly spaced near the body. Both equilibrium-air and perfect-gas models were used. Figure 11 shows the results. Although the pressure distributions do change very slightly (about the width of the curve in the figure over a small portion of the body length), it is clear that for low-drag shapes viscous effects are minor. However, there remains a possibility that a variation of transition location with power-law exponent could have a significant effect on drag.

Thermodynamic Gas-Model Effects

The validity of the calorically perfect gas model must be examined for the Mach numbers used in this study. Results from CFL3D using both the calorically perfect gas and the equilibrium-air models were compared to assess the importance of real-gas effects. Drag coefficient results are given in Table 2 and show that minimal gas-model effects are found for low-drag bodies. The calculations were carried out using

Table 2 Comparison of drag coefficients between perfect-gas and the equilibrium-air models

M_∞	Inviscid calculation, $n = 0.75$		PNS calculation,[a] $n = 0.69$	
	Perfect gas	Equilibrium air[b]	Perfect gas	Equilibrium air[b]
6.28	0.053070	0.053063 (0.013%)		
8.00	0.049987	0.049981 (0.012%)	0.057683	0.057867 (0.32%)
12.0	0.046350	0.046349 (0.002%)		

[a]Adiabatic wall temperature boundary condition.
[b]Percent diferences from perfect gas are given.

$n = 3/4$ for the inviscid analysis and $n = 0.69$ for the PNS analysis. The equilibrium calculations were carried out for conditions corresponding to an altitude of 96,000 ft.

Pressure distributions are shown in Fig. 12. Differences between the pressure distributions obtained using the two different gas models cannot be identified. Although the pressures are nearly identical, the surface temperature is affected, as shown in Fig. 13. Near the nose a difference of from 50 K at $M_\infty = 6.28$ to nearly 600 K at $M_\infty = 12$ was found. This is not surprising based on an examination of the typical effects on pressure of various thermodynamic models for air.[19,20]

Numerical Examination of the Nose Region

Results presented thus far have ignored the explicit effect of the nose bluntness. Recalling the small scale of the bluntness compared with the rest of the geometry as shown in Fig. 2, normal numerical solution grids do not "see" the bluntness. To assess the effect of bluntness, calculations were made using the global-iteration scheme of CFL3DE and including nose bluntness explicitly. The resulting pressure distribution over the entire body is presented in Fig. 14 and compared with the space-marching results. No difference can be identified. The shock locations are shown in Fig. 15, and a very small effect was found.

These results show that the bluntness of the minimum-drag power-law bodies considered is confined to such an extremely small region that the detailed treatment of the nose bluntness and the resulting entropy layer is not necessary to obtain valid results for the pressure distribution over the entire body.

Hayes Forebody Shape

The so-called Hayes body was also evaluated. Figure 16 presents the Hayes minimum-drag body shape compared with the optimum ($n = 0.69$) power-law body and the classic 3/4 body. Even though this body begins with a power-law shape of 3/4, the value of the coefficient of x^n produces a shape that closely corresponds to the $n = 0.69$ power-law body determined earlier to be optimum over the initial part of the body. Initially, the Hayes shape is larger than the other shapes and then rather abruptly bends to meet the specified maximum diameter requirement. This effect is clearly shown in the pressure distribution, also shown in Fig. 16, plotted with negative C_p upward. As expected, the body is initially similar to the $n = 0.69$ case; then due to its shallow slope the pressure is lower than the other shapes.

The drag of the Hayes body was included in Fig. 9. At $M_\infty = 6.28$ for the same given length and diameter, the Hayes shape has 4.95% more drag than the $n = 0.69$ power-law body. The same trend is observed at Mach 8. Thus the Hayes shape appears to offer no advantage for the problem of a given length and diameter. It has more volume, and this appears to result in a higher drag.

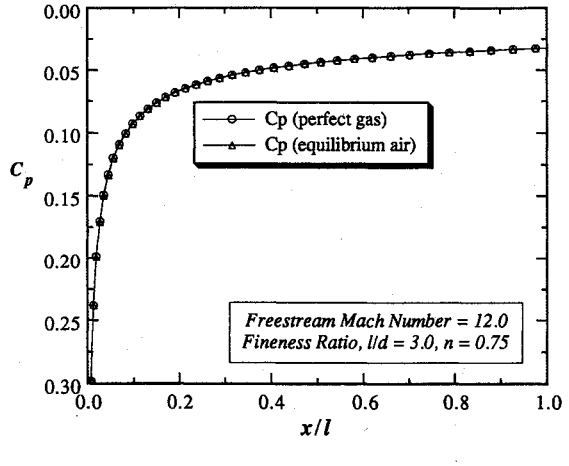

Fig. 11 Pressure and skin-friction distribution for the optimum power-law shape ($n = 0.69$, adiabatic wall B.C. was used for PNS calculation).

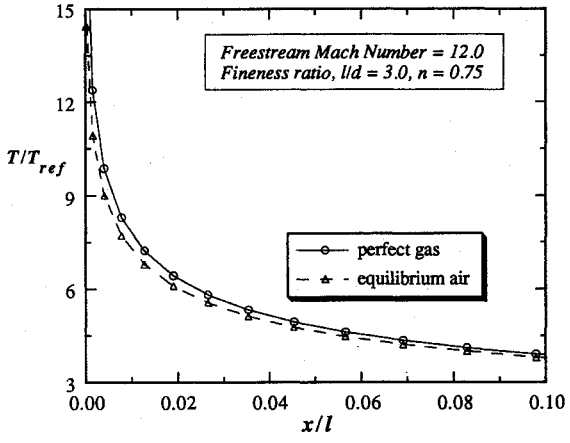

Fig. 12 Comparison of pressure distributions of perfect gas and equilibrium air.

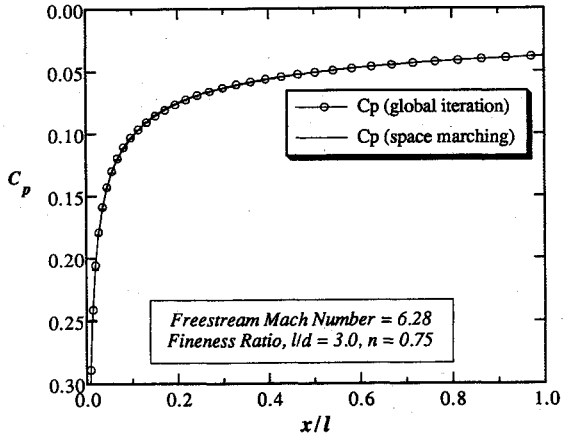

Fig. 13 Comparison of temperature distributions between perfect gas and equilibrium air.

Discussion of Results

To summarize our findings, Fink's figure is repeated as Fig. 17 with the results obtained in the present study included. It is clear that an analysis with an advanced code verifies the trends previously obtained. However, CFL3DE predicts drag values for the $n = 0.69$ power law slightly below the values obtained previously for other shapes in this Mach number regime. The validity of the Fink analysis is shown for high Mach numbers. The breakdown of the assumptions of the hypersonic small-disturbance theory is evident at the lower Mach numbers. The

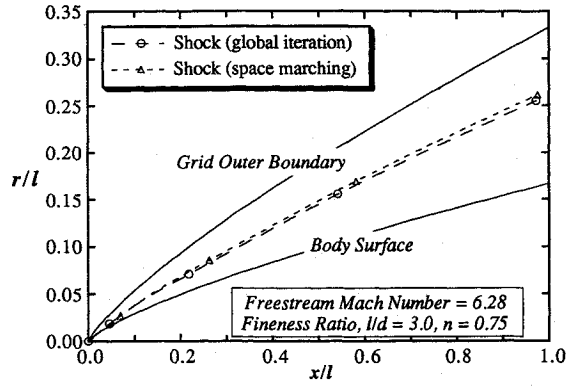

Fig. 14 Comparison of pressure distributions for different numerical schemes.

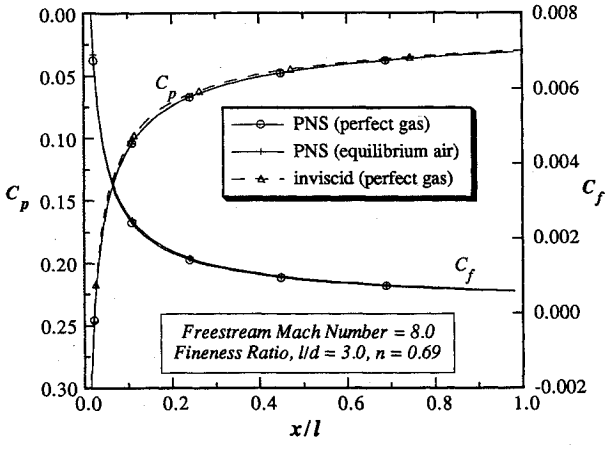

Fig. 15 Comparison of the shock locations for the different numerical schemes.

importance of using a complete analysis, such as CFL3DE, is clearly demonstrated.

Despite the apparent closeness of the results for the $n = 0.69$, 0.75, and 0.65 bodies, the differences in drag are significant. Recall that in the classic case of the F-102 aircraft the benefits from area ruling on the order of 25 counts meant the difference between subsonic and supersonic flight. Thus designers should exploit the extra benefits of the $n = 0.69$ body.

Conclusions

Computations using the CFL3DE and CFL3D codes for Mach numbers 3–12 lead to these conclusions:

1) The optimum power law is $n = 0.69$, virtually independent of Mach number for the $l/d = 3$ case considered. For $l/d = 5$ the minimum changes slightly, occurring at $n = 0.70$.

2) The calorically and thermally perfect gas model produces the same results as the equilibrium-air model for the low-drag bodies studied over a Mach range up to $M_\infty = 12$. This result, although not surprising to workers in the field, has apparently not been well documented.

3) The body shape proposed by Hayes has a higher drag than the optimum power-law body.

These results provide a necessary foundation for future work on advanced three-dimensional minimum-drag shapes for supersonic and hypersonic flight vehicles.

Acknowledgment

We would like to acknowledge R. W. Walters of the Virginia Polytechnic Institute and State University for providing us with access to CFL3DE and CFL3D and for consulting with us on the use of the code for this work.

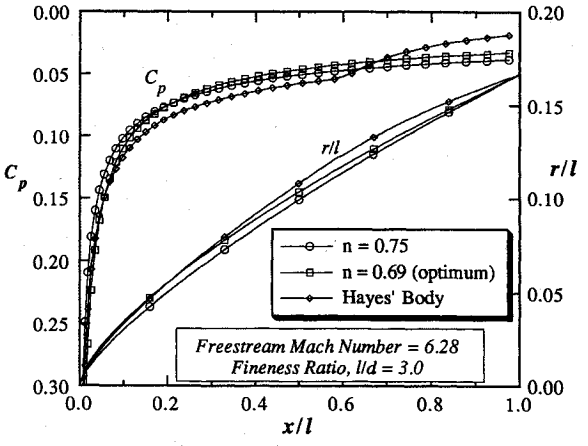

Fig. 16 Comparison of power-law shapes and pressure distributions with the Hayes body shape.

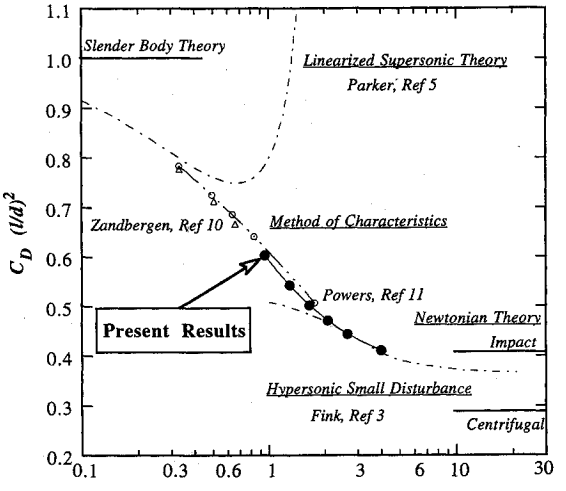

Fig. 17 Results of current study added to the Fink[3] chart.

References

[1]Harris, R. V., Jr., "On the Threshold—The Outlook for Supersonic and Hypersonic Aircraft," AIAA Paper 89-2071, Aug. 1989.

[2]Miele, A. (ed.), *Theory of Optimum Aerodynamic Shapes*, Academic, New York, 1965.

[3]Fink, M. R., "Hypersonic Minimum-Drag Slender Bodies of Revolution," *AIAA Journal*, Vol. 4, No. 10, 1966, pp. 1717–1724.

[4]Hahne, D. E., Luckring, J. M., Covell, P. F., Phillips, W. P., Gatlin, G. M., Shaughnessy, J. D., and Nguyen, L. T., "Stability Characteristics of a Conical Aerospace Plane Concept," Society of Automotive Engineers, Warrendale, PA, SAE Paper 892313, Sept. 1989.

[5]Parker, H. M., "Minimum-Drag Ducted and Pointed Bodies of Revolution Based on Linearized Supersonic Theory," NACA Rept. 1213, 1955.

[6]Eggers, A. J., Jr., Resnikoff, M. M., and Dennis, D. D., "Bodies of Revolution Having Minimum-Drag at High Supersonic Speeds," NACA Rept. 1306, 1957.

[7]Hayes, W. D., and Probstein, R. F., *Hypersonic Flow Theory*, Academic, New York, 1959, pp. 103–106.

[8]Miele, A., "A Study of Slender Shapes of Minimum-Drag Using the Newton-Busemann Pressure Coefficient Law," *AIAA Journal*, Vol. 1, No. 1, 1963, pp. 168–178.

[9]Cole, J. D., "Newtonian Flow Theory for Slender Bodies," *Journal of the Aerospace Sciences*, Vol. 24, No. 6, 1957, pp. 448–455.

[10]Zandbergen, P. J., "On the Determination of Optimum Shapes with Finite Nose Angles," National Aero- and Astronautical Research Inst., Report NLR-TR G.30, Amsterdam, The Netherlands, July 1964.

[11]Powers, S. A., "Drag Minimization Using Exact Methods,"

AIAA Journal, Vol. 2, No. 5, 1964, pp. 941–943.

[12]Maestrello, L., and Ting, L., "Optimum Shape of a Blunt Forebody in Hypersonic Flow," NASA CR 181955, Dec. 1989.

[13]Stivers, L. B., Jr., and Spencer, B., Jr., "Studies of Optimum Body Shapes," *Conference on Hypersonic Aircraft Technology*, NASA SP-148, May 1967, pp. 87–101.

[14]Perkins, E. W., Jorgensen, L. H., and Sommer, S. C., "Investigation of the Drag of Various Axially Symmetric Nose Shapes of Fineness Ratio 3 for Mach Numbers from 1.24 to 7.4," NACA Rept. 1386, 1958.

[15]Spencer, B., Jr., and Fox, C. H., Jr., "Hypersonic Aerodynamic Performance of Minimum-Wave-Drag Bodies," NASA TR R-250, July 1966.

[16]Fournier, R. H., Spencer, B., Jr., and Corlett, W. A., "Supersonic Aerodynamic Characteristics of a Series of Related Bodies with Cross-Sectional Ellipticity," NASA TN D-3539, Aug. 1966.

[17]Thomas, J. L., van Leer, B., and Walters, R. W., "Implicit Flux-Split Schemes for the Euler Equations," AIAA Paper 85-1680, July 1985.

[18]Huebner, L. D., Pittman, J. L., and Dilley, A. D., "Hypersonic Parabolized Navier-Stokes Code Validation on a Sharp Nose," *Journal of Aircraft*, Vol. 26, No. 7, 1989, pp. 650–656.

[19]Grossman, B., and Walters, R. W., "An Analysis of Flux-Split Algorithms for Euler's Equations with Real Gases," AIAA Paper 87-1117, June 1987.

[20]Walters, R. W., Cinnella, P., Slack, D. C., and Halt, D., "Characteristic-Based Algorithms for Flows in Thermo-Chemical Nonequilibrium," AIAA Paper 90-0393, Jan. 1990.